The 2012 World Congress on
Advances in Civil, Environmental, and Materials Research (ACEM' 12)
Seoul, Korea, August 26-30, 2012

Numerical Simulation on Fluid-structure Interaction of Wind around Supper-tall Building at High Reynolds Number Conditions

* Shenghong HUANG [1)], Rong LI [2)], Q.S.Li [3)]
[1),2)] *School of Engineering Science, University of Science and Technology of China, Hefei, 230026, P.R. China, hshnpu@ustc.edu.cn*
[3)] *Dept. of Building and Construction, City University of Hong Kong, Kowloon, Hong Kong, bcqsli@cityu.edu.hk*

ABSTRACT

With more and more high-rise building being constructed in recent decades, bluff body flow with high Reynolds number and large scale dimensions has become an important topic in theoretical researches and engineering applications. In view of mechanics, the key problems in such flow are high Reynolds number turbulence and fluid-solid interaction. Aiming at such problems, a parallel fluid-structure interaction method based on socket parallel architecture was established and combined with the methods and models of large eddy simulation developed by authors recently. The new method is validated by the full two-way FSI simulations of 1:375 CAARC building model with Re=70000 and a full scale Taipei101 high-rise building with Re=1e8, The results obtained show that the proposed method and models is potential to perform high-Reynolds number LES and high-efficiency two-way coupling between detailed fluid dynamics computing and solid structure dynamics computing so that the detailed wind induced responses for high-rise buildings can be resolved practically.

1. INTRODUCTION

With more and more high-rise buildings being constructed in recent decades, there are increasing academic and engineering interests upon the interaction of wind and high-rise building structures. In fact, with the increase of building height, the natural vibration frequencies are deceasing, which may be close to the predominant frequencies of the strong/typhoon dynamic loads. Therefore, the tall buildings may exhibit significant wind-induced responses under the effect of strong/typhoon dynamic loads. These wind-induced responses are becoming the crucial factors in determining the safety and comfort of high-rise buildings.

In view of mechanics, interaction between wind and high-rise buildings are fluid-structure interaction problems (FSI) in essence. Up to now, many published literatures have discussed FSI problems of high-rise building. In this paper, numerical works based on application of computational fluid dynamics (CFD) as well as computational structure dynamics (CSD) are discussed.

[1)] Associate Professor

[2)] graduate

In fact, benefiting from advancing of computational mechanics and computer hardwares, CFD and CSD have been widely used in simulating the wind loads and wind effects on various buildings and structures in wind engineering, and there always exist a trend to deal with FSI problems with coupled CFD/CSD methods. Tamura et al (1997;1999a;1999b;2003) may be the first to tackle this problems by using CFD based on large eddy simulation (LES) and moving mesh techniques, they successfully captured several typical aeroelastic movements of 2D cylinders. However, their CSD analysis was only based on 1D model. Works with similar methods include Su et al. (2008), Kataoka et al. (2008), Revuz et al.(2009), and Braun et al. (2009) recently. In the work of Revuz et al. and Braun et al., an arbitrary Lagrangian Eulerian (ALE) technique was introduced to deal with moving and deforming mesh of CFD, while Braun et al. considered the geometrically nonlinear effects by employing a Generalized-α model in the time domain. With the development of commercial CFD and CSD software, more works based on commercial soft are proposed, such as the work of Swaddiwuhipong et al. (2002), Fang and Gu (2008). However, most of them are only based on Reynolds-averaged Navier-Stokes (RANS) simulations or simple CSD computations. In general, the common features of those studies can be summarized as following: (1) Both CFD and CSD models are based on governing equations and dynamic principle of physics, therefore relative complete wind loads and structure movements information can be obtained; (2) Coupling between CFD and CSD, i.e. FSI, is required, which may involve complicated mesh match and interface movement of CFD and CSD, since different mesh and discretization method are adopted by CFD and CSD respectively. However, according to previous works reviewed above, full two-way coupling between 3D CFD and 3D CSD are still rare, and besides, most previous works focus on scaled and relative simple geometry model (1/300 square cylinder etc.) as well a simplified CSD computation.

In this paper, a parallel fluid-structure interaction method based on socket parallel architecture was established. The target of such method is to realize high-efficiency two-way coupling between detailed fluid dynamics computing and solid structure dynamics computing so that the detailed fluid induced responses, which are key for structure safety and comfort evaluation, can be resolved practically. Besides, several models and methods for high Reynolds number LES of CFD proposed recently by authors have also been combined together so that the FSI problem of wind around large scale structures at high Reynolds number conditions can be evaluated practically.

2. METHODS AND ALGORITHM

As summarized by Tamura (2008), practical use of LES in wind engineering should resolve three key issues: (1) Generation of inflow turbulence; (2) Sophisticated sub-grid scale (SGS) turbulence modeling; (3) Numerical discretization with conservation of various physical quantities for modeling complex geometries. It is appealing for more advances on LES methods as well as their applications in CWE. In the recent studies of the authors, a general inflow turbulence generation method (Huang et al., 2010a) and a new

dynamic one-equation subgrid-scale (SGS) model of LES (Huang and Li, 2010b) were developed under such motivations.

2.1 Inflow turbulence generation method

Currently, there are two kinds of inflow turbulence generation methods. The first method is to numerically simulate turbulent flows in an auxiliary computational domain and the other method provides generation of inflow turbulence by artificial numerical models. The presented general inflow turbulence generator for LES is based on discretizing and synthesizing of random flow generation (DSRFG) technique (Huang et al., 2010a), which belongs to the second kind of method. The method was proved to be able to generate a fluctuating turbulent flow field satisfying desired spectra and spatial correlations including inhomogeneity and anisotropy. In addition, it has built-in divergence-free mechanism in random velocity generation, thus no velocity correction and preliminary storage for time-sequential data are needed. The detailed derivation of the DSRFG method is given by Huang and Li (2010a), and a brief formulation of the method is presented below:

$$\mathbf{u}(\mathbf{x},t)=\sum_{m=k_0}^{k_{\max}}\mathbf{u}_m(\mathbf{x},t)=\sum_{m=k_0}^{k_{\max}}\sum_{n=1}^{N}\left[\mathbf{p}^{m,n}\cos(\tilde{\mathbf{k}}^{m,n}\cdot\tilde{\mathbf{x}}+\omega_{m,n}t)+\mathbf{q}^{m,n}\sin(\tilde{\mathbf{k}}^{m,n}\cdot\tilde{\mathbf{x}}+\omega_{m,n}t)\right] \quad (1)$$

where $\mathbf{p}^{m,n}=\dfrac{\boldsymbol{\varsigma}\times\mathbf{k}^{m,n}}{\left|\boldsymbol{\varsigma}\times\mathbf{k}^{m,n}\right|}\sqrt{a\dfrac{4E(k_m)}{N}}$, $\mathbf{q}^{m,n}=\dfrac{\boldsymbol{\xi}\times\mathbf{k}^{m,n}}{\left|\boldsymbol{\xi}\times\mathbf{k}^{m,n}\right|}\sqrt{(1-a)\dfrac{4E(k_m)}{N}}$, $\tilde{\mathbf{x}}=\dfrac{\mathbf{x}}{L_s}$,

$\tilde{\mathbf{k}}^{m,n}=\dfrac{\mathbf{k}^{m,n}}{k_0}$, $\left|\mathbf{k}^{m,n}\right|=k_m$, $\omega_{m,n}\in N(0,2\pi k_m)$, $\boldsymbol{\varsigma}$ and $\boldsymbol{\xi}$ are vector form of ς_i^n and ξ_i^n, respectively, and $\varsigma_i^n,\xi_i^n\in N(0,1)$. k_m is wave number. L_s is turbulence integral length scale which is an important parameter used as the scaling factor for spatial correlation. a is a random number uniformly distributed between 0~1. $N=100\sim200$ (sampling number for each wave number k_m) are found to be accurate enough and economical for most applications in wind engineering. Fig.1(a) shows comparison of longitudinal fluctuating velocity spectra simulated by the DSRFG method and RFG method proposed by Smirnov(2001). It is clear that the spectrum determined by the DSRFG method agrees with the von Karman spectrum well, while the spectrum obtained by the RFG method decays too fast in the inertial sub-range.

2.2 Dynamic one-equation subgrid-scale model for large eddy simulations

Up to now, the development of SGS models for LES has experienced three stages, namely, the algebraic eddy viscosity models, one-equation eddy viscosity models and two-equation eddy viscosity models. The aim of such developments is to accurately model the SGS and the energy transfer mechanism with GS (grid-scale) for high Reynolds number flows. So, it is necessary and significant to develop a SGS model that is engineering-oriented and is capable of solving some practical engineering problems effectively. As

introduced previously, the authors developed a new dynamic one-equation subgrid-scale (SGS) model for LES (Huang and Li, 2010b) which combines the advantages of both the dynamic one-equation SGS model (Kajishima and Nomachi, 2006) and the WALE model (Nicoud and Ducras,1999). and a brief formulation of the model is presented below:

The governing equations of LES for incompressible flow are obtained by conducting the grid filtering operation to the Navier-Sokes (NS) equation and continuity equation. The filtered continuity equation and the NS equation are expressed as

$$\frac{\partial \overline{u}_i}{\partial x_i} = 0 \tag{2}$$

$$\frac{\partial \rho \overline{u}_i}{\partial t} + \frac{\partial \left(\rho \overline{u}_i \overline{u}_j \right)}{\partial x_j} = -\frac{\partial}{\partial x_i}\left(\overline{p} + \frac{2}{3}\rho k_{sgs} \right) + \frac{\partial}{\partial x_j}\left[2\rho(\upsilon_s + \upsilon)\overline{S}_{ij} \right] \tag{3}$$

where $\overline{u}_i$ denotes the GS component of velocity, $\overline{p}$ represents the GS component of pressure, ρ denotes the fluid density, υ is the kinetic viscosity of fluid, υ_s is the SGS eddy viscosity, given by

$$\upsilon_s = C_v \Delta_v \sqrt{k_{sgs}} \tag{4}$$

Here C_v is regarded as a constant instead of a dynamical parameter, as suggested by Kajishima and Nomachi (2006). Δ_v is the characteristic length, and k_{sgs} is the SGS kinetic energy. According to Okamoto and Shima (1999), Δ_v is calculated by

$$\Delta_v = \frac{\overline{\Delta}}{1 + C_k \dfrac{\overline{\Delta}^2 \overline{S}^2}{k_{sgs}}} \tag{5}$$

The above equation is used here to meet the correct asymptotic behavior to a wall, in which C_k is a model constant, $\overline{S} = \sqrt{2\overline{S}_{ij}\overline{S}_{ij}}$. Since both C_v and Δ_v are non-negative values, υ_s cannot take a negative value, thus computation of Eq.(3) is expected to be numerically stable.

k_{sgs} is obtained from a transportation equation below:

$$\frac{\partial k_{sgs}}{\partial t}+\frac{\partial \overline{u}_j k_{sgs}}{\partial x_j}=-\tau_{ij}\overline{S}_{ij}-C_\varepsilon\frac{k_{sgs}^{3/2}}{\overline{\Delta}}+\frac{\partial}{\partial x_j}\left[\left(C_d\Delta_v\sqrt{k_{sgs}}+\upsilon\right)\frac{\partial k_{sgs}}{\partial x_j}\right]-\varepsilon_w \tag{6}$$

And $-\tau_{ij}\overline{S}_{ij}$ in Eq.(6) is constructed by

$$-\tau_{ij}\overline{S}_{ij}=\left(\left(C_W^*\overline{\Delta}\right)^2\frac{\left(S_{ij}^d S_{ij}^d\right)^{\frac{3}{2}}}{\left(\overline{S}_{ij}\overline{S}_{ij}\right)^{\frac{5}{2}}+\left(S_{ij}^d S_{ij}^d\right)^{\frac{5}{4}}}\right)\left|\overline{S}\right|^2-\frac{2}{3}k_{sgs}\delta_{ij}\overline{S}_{ij} \tag{7}$$

where

$$S_{ij}^d=\frac{1}{2}\left(\overline{g}_{ij}^2+\overline{g}_{ji}^2\right)-\frac{1}{3}\delta_{ij}\overline{g}_{kk}^2 \tag{8}$$

$$\overline{g}_{ij}=\frac{\partial\overline{u}_i}{\partial x_j} \tag{9}$$

$$C_W^*=\begin{cases}C_W\dfrac{\left|\overline{\Omega}\right|}{\left|\overline{S}\right|} & when \quad \dfrac{\left|\overline{\Omega}\right|}{\left|\overline{S}\right|}<1\\ C_W & when \quad \dfrac{\left|\overline{\Omega}\right|}{\left|\overline{S}\right|}\geq 1\end{cases} \tag{10}$$

There are several advantages related to this formulation:

All the turbulence structures related to kinetic energy dissipation can be detected by $S_{ij}^d S_{ij}^d$ without the test filtering operation. $S_{ij}^d S_{ij}^d$ behaves like y^2 near wall, which guarantees the production term going naturally to zero (y^3) in the vicinity of a wall so that neither (dynamic) constant adjustment nor damping function is needed to compute wall bounded flows. $S_{ij}^d S_{ij}^d=0$ in case of pure shear flow, produces zero production of k_{sgs}. Thus, it is possible to reproduce the laminar to turbulent transition process through the growth of linear unstable modes.

It is worthy noting that using the velocity gradient tensor $\overline{g}_{ij}$ to construct the operator S_{ij}^d for calculating SGS viscosity dynamically was firstly introduced by Nicoud and Nucros (1999) in their WALE model. In our newly developed SGS model, the dynamic mechanism of the WALE model was introduced into the OD model by Eq.(6), which combines both advantages of the OD model and the WALE model.

Fig.2 shows a validation results of flow past a square cylinder at a Reynolds number of 22000, while the results of another one-equation SGS

model named LDKM (Kim and Menon,1995) are also presented for comparison purposes. The comparative study results show that the proposed model is of less grid dependence and has a potential of wide applications in complex geometries and high Reynolds number turbulent flows.

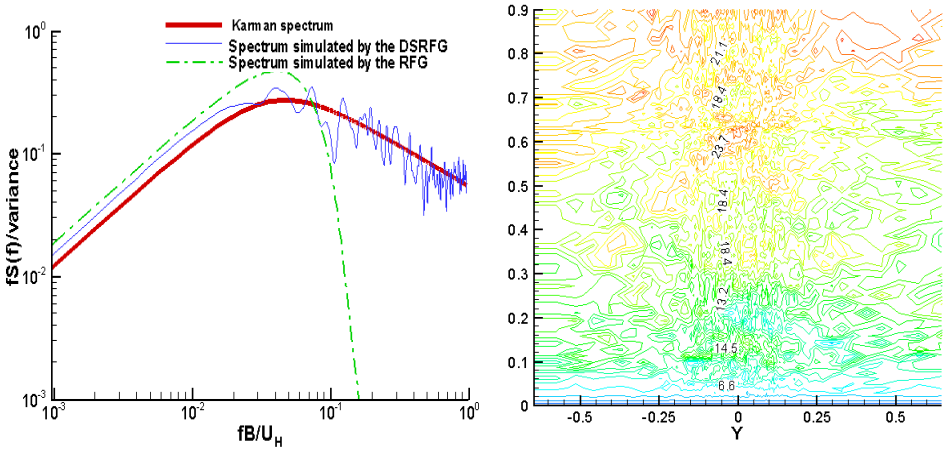

Fig.1. Inflow turbulence generated by DSRFG. (a) spectra; (b) instantaneous velocity contour

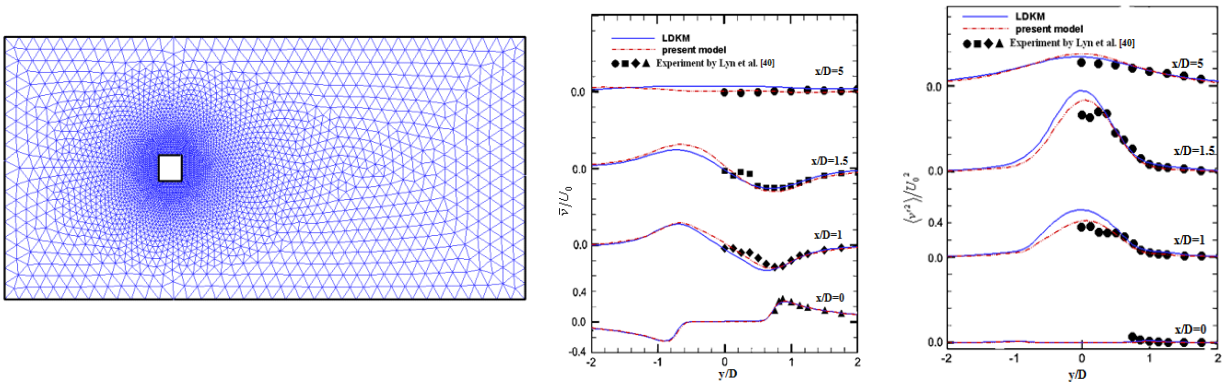

(a) (b) (c)

Fig. 2 A validation example for the new SGS model. (a) A coarse unstructured grid; (b) Time-averaged transverse velocity comparison; (c) Time-averaged transverse normal stress comparison.

2.3 A parallel fluid-structure interaction method based on socket parallel architecture

As discussed previously, FSI may involve complicated mesh match and interface movement of CFD and CSD, since different mesh and discretization method are adopted by CFD and CSD respectively. And besides, CFD and CSD are often programmed into different code and packages, which leads to some difficult to conduct two-way coupling. In present investigation, a parallel two-way fluid-structure interaction method based on socket parallel architecture is established. As shown in Fig.3, the coupling process is performing as follows:

(1) To conduct CFD computation, then the wind loads is obtained.

(2) To integral the wind loads along height layer by layer, i.e., F_x^i (along wind force), F_y^i (across wind force) and M_z^i (torsional moment) for each layer are obtained.

(3) A message is written with F_x^i , F_y^i and M_z^i, then the message is transferred to CSD through socket communication.

(4) Once F_x^i , F_y^i and M_z^i are obtained, the CSD solver begin to conduct CSD computation, the response information such as displacement is obtained.

(5) To obtain the response information along height layer by layer, i.e., U_x^i ,U_y^i ,U_z^i (x, y, z direction displacement respectively) and Rot_x^i, Rot_y^i ,Rot_z^i (x, y, z direction rotation angle respectively), by integral the out wall displacement information layer by layer.

(6) A message is written with U_x^i ,U_y^i ,U_z^i,Rot_x^i, Rot_y^i ,Rot_z^i, then the message is transferred back to CFD through socket communication.

(7) Updating the surface mesh of target building in CFD solver according to U_x^i ,U_y^i ,U_z^i,Rot_x^i, Rot_y^i ,Rot_z^i, then repeat above procedures.

It is worthy to noting that:

(1) Different from ordinary two way coupling method, in which all datasets of FSI interface including pressure and displacement node by node are exchanged between CFD and CSD, only integrated information of FSI interface is exchanged in proposed method, leading to greatly promotion of FSI efficiency.

(2) For high-rise building, the deformation by wind loads mainly occurs along height globally, while the local deformation for each layer can be neglected, which makes the integration of information on FSI interface layer by layer reasonable.

(3) Socket message transferring method makes the FSI method possessing the capability of coupling on heterogeneous platforms.

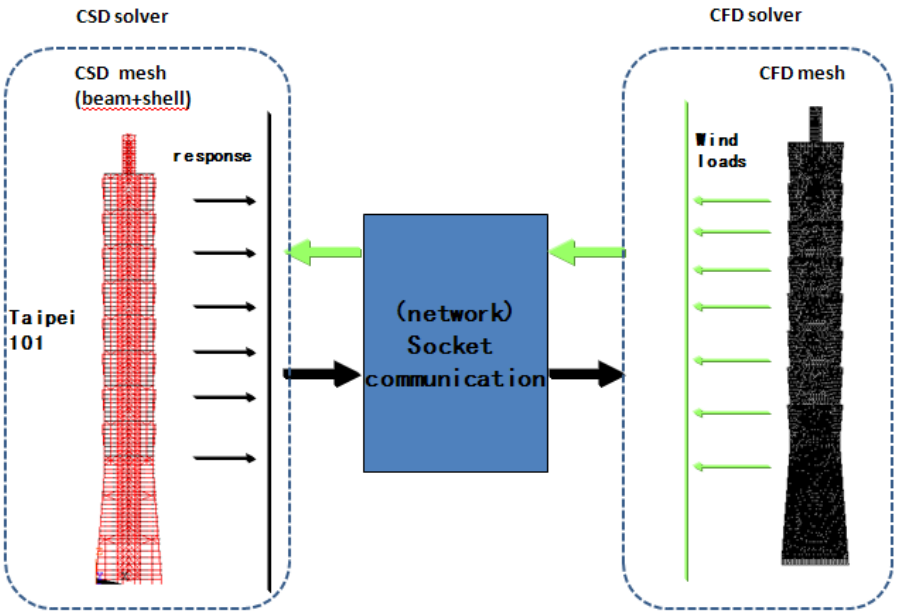

Fig.3 A parallel two-way FSI method based on socket architecture

3. RESULTS AND DISCUSSION

3.1 Calibration of FSI method on standard CAARC building model with Re=70000

To validate the FSI method proposed in this paper, numerical simulation of wind flow past a 1:375 CAARC building model is conducted firstly. The Reynolds number based on the approaching mean speed U_H and model width W is about 70, 000. The boundary conditions and main computational parameters for both CFD and CSD in this case are listed in Table.1. As shown in Table.1, there are three characteristics in present case:

(1) Different operating platforms are adopted by CFD solver and CSD solver respectively, which is beneficial form socket communication mechanism.

(2) Different mesh styles are adopted by CFD and CSD solver respectively, which is a virtue of present FSI method.

(3) Unlike most reported aeroelastic experiments, the constraint of CSD in present numerical simulation is set as a full elastic state, i.e. elastic body with a stiff base. The aim of present setup is to check the deforming consistency of CFD and CSD mesh in physical state.

(4) Noting that a low Young's modulus for structure is adopted in CSD, aiming to obtain a relative large deforming size in simulation so that the dynamic mesh method for large deforming situation can be checked rigorously.

Fig.4 shows the velocity contour with mesh movement of both CFD (black) and CSD (red) as well as the monitored displacements at the top of building. Fig.5 shows force history and its spectra density in present FSI simulation and

as a comparison, the results of case without FSI are also shown. It is obviously observed that:

(1) The CFD mesh nodes on the building surfaces move and deform accordantly with nodes of beam189 elements on the vertical center line of building body, indicating a right loads and response information exchange in present FSI method.

(2) According to the monitored displacements at the top of building, the along-wind structural response with large amplitudes is observed initially, and then is damped gradually to small amplitudes, which should be due to the combined action of the aerodynamic damping and structural damping. While for across-wind structural response, on the contrary, a continuous increasing of amplitude until 3s is observed, which should be caused by the synchronizing of structural and vortex shedding frequencies. In fact, the reduced velocity of present FSI case is about 10, which is very close to the lock-in velocity (11.1m/s) according to previous experimental works (Thepmongkorn et al., 1999;Melbourne ,1980).

(3) In the plots of forces and their spectra comparisons, some discrepancy between cases with and without FSI is observed. A typical feature is the frequency of peak spectral density is shifted towards natural frequency of structure, owing to the coupled FSI mechanism.

To further validate the CFD/CSD results, Fig.6 shows the comparison of along-wind and across-wind normalized displacements as functions of the reduced velocity with available experimental and numerical data. As shown in Fig.6, the results of present work are generally in agreement with experimental and numerical data. The discrepancy may be caused by a too low Young's modulus of CSD was adopted in present work.

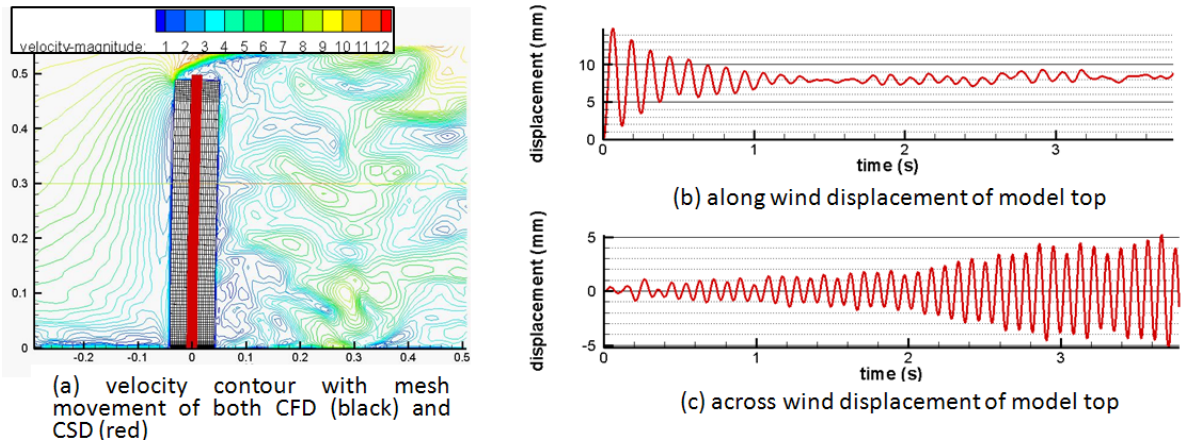

(a) velocity contour with mesh movement of both CFD (black) and CSD (red)

(b) along wind displacement of model top

(c) across wind displacement of model top

Fig. 4 Wind-structure interaction simulation of CAARC model

Table.1 The boundary conditions and computational parameters

	CFD	CSD
Solver	Fluent 6	Ansys 12
Platform	linux	windows
Numerical model	LES new one-equation SGS model DSRFG inflow generation method dynamic mesh Noted： New SGS model and DSRFG are implemented with UDF technique	Full transient analysis large displacement option, Ramped loading
Mesh style	Hybrid	Beam189
Boundary condition	VH=9.6m/s, H=0.487m, power law with α=0.29	Full constraint to end on the ground
Solution Constants	Specific mass ρ1.2 kg/m3 Dynamic viscosity 1.46e-5 N.m/s2 Characteristic dimension 121.2mm	Specific massρ 60kg/m3, Young's modulus E 1.3Mpa Poisson's ratio 0.25 Natural frequency 7.96Hz Damping ratio to critical 0.01

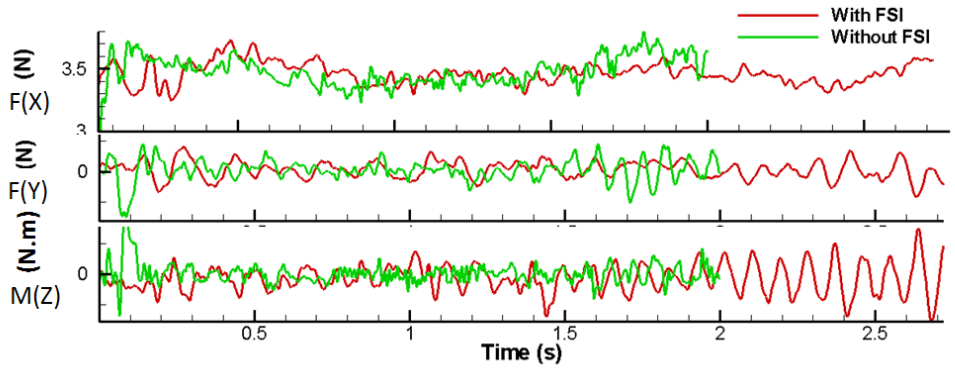

(a) Force comparison between cases with and without FSI

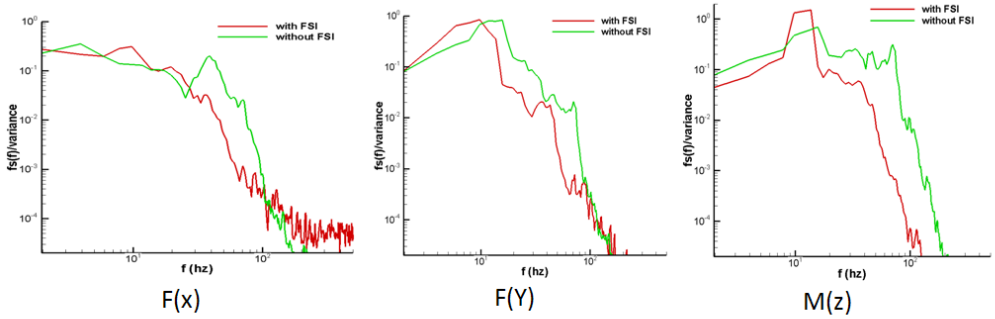

(b) Spectral density comparison between cases with and without FSI

Fig. 5 Comparison of force and its spectra density between cases with and without FSI

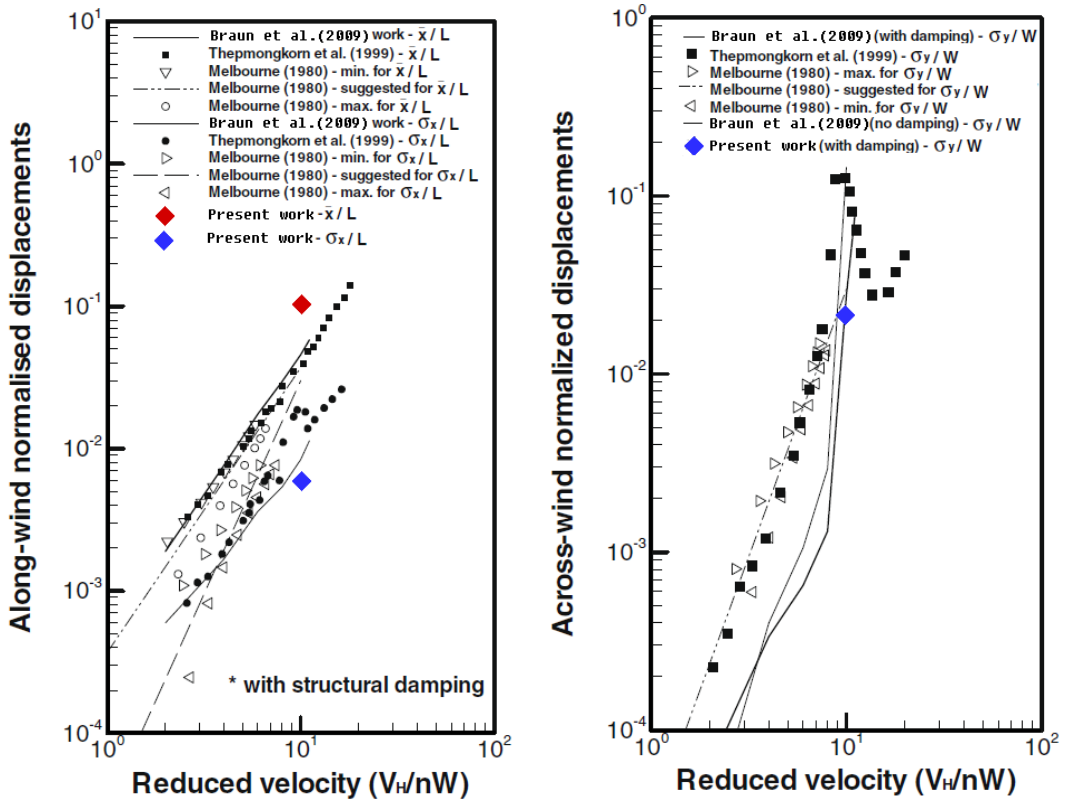

Fig. 6 Comparison of along-wind and across-wind normalized displacements as functions of the reduced velocity with available data

3.2 FSI simulation on Taipei101 building with Re=1e8

With the validated methods addressed in last section, the wind effects on Taipei 101 Tower are also evaluated. As shown in Fig.7(a), Taipei 101 Tower is a 101-floor and 508 m high landmark skyscraper located in Xinyi District of Taipei, Taiwan.

Fig.7 (b) shows its surface mesh of CFD. The computational domain of CFD covers 33Db (Db is the width of the building base, which is 62.4m) in streamwise (X) direction (-9.5<x/Db<23.5), 17 Db in lateral or normal (Y) direction (-8.5<y/Db<8.5) and 2 H in vertical (Z) direction, with a hybrid mesh arrangement and about 5.5×106 cells.

Fig.7 (c) shows its mesh of CSD, It is a 3D finite-element FE model of Taipei 101 Tower structure, which was established based on the structural design drawings. Four kinds of elements were employed in establishing the FE model: 12-nodes 3D beam elements (columns and beams), 3D link elements (braces), Mass elements (live loads and nonstructural components), shell elements (floors). The connection between the structure and its foundation was treated to be fixed. Mode analysis shows that the first order natural frequency is about 0.16 Hz for present FEM model, which is close to the measured value (0.156) by Li et al. during Typhoon Matsa.

The boundary conditions for CFD are set as follows: The inlet mean wind speed profile in the boundary layer of atmosphere is assumed to follow a power law, with U_{10} =43.27m/s and exponent of 0.15(Rowan Williams Davies & Irwin Inc,1999). The turbulence parameters are in the range from 0.18 to 0.23, based on field measurement of Shiau (2000) and Li et al (2005).

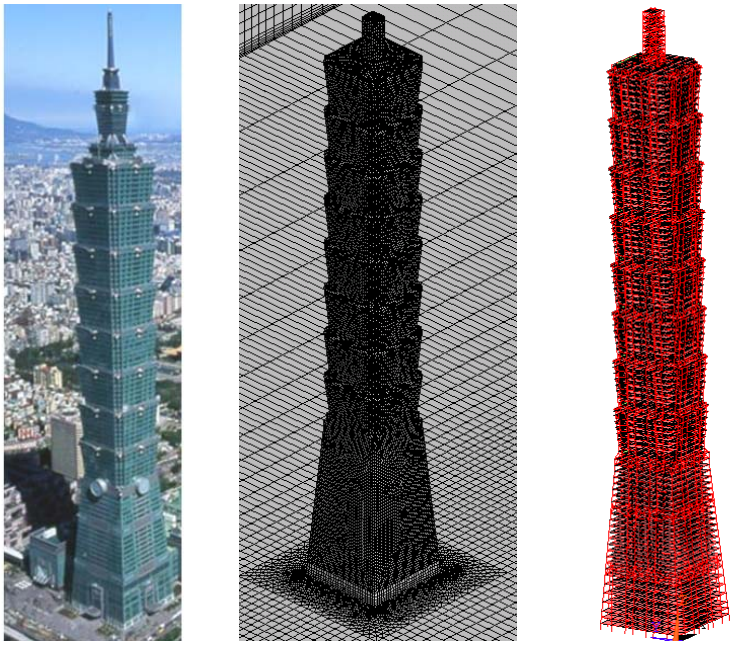

(a) prototype (b) CFD mesh (c) CSD mesh

Fig.7 Taipei101 building prototype and its CFD and CSD model

Fig.8 shows the matched mesh of CFD and CSD during the computations of FSI, in which the red dot represent the FEM node of CSD while the black one represent the CFD node. It is clear that both nodes of CFD and CSD on the building surfaces move accordantly with each other, indicating a matched state on the interface of fluid and structure.

Fig.9 further shows the coupled fluid contours and structure movement during the computations of FSI, in which a strong vortex shedding is observed with the moving of structure.

The wind loads data obtained with present FSI simulation are listed in Table.2. The data obtained by RWDI(1999) with wind tunnel experiments are also listed for comparison purpose. It is clear that the results of present work agree with the wind tunnel test data generally, but about 30~40% under-prediction of rms values are also observed.

Fig.10 further shows the along-wind and across-wind normalized displacements at the top of Taipei101 tower as a function of reduced velocity. The available experimental and numerical data of CAARC are also plotted for reference. It should be noted that the geometry and structure of Taipei101 are very different from that of CAARC building, so the data of CAARC can only be

treated as reference values. Anyway, It is reasonably to observed that the results of along wind and across-wind normalized displacements of Taipei101 (V_H=7.5m/s) falls in region of plots covered by those experimental and numerical data.

Fig.11 shows the spectra comparison of acceleration at the top of Taipei101 tower with that measured by Li et al (2011). They agreed well with each other in frequency range of 0~0.5Hz, indicating a correct response of present CFD/CSD simulation.

Table .2 Comparison of wind loads with wind tunnel test data

	$\overline{F_D}$	$F_{D,\min}$	$F_{D,\max}$	$\overline{F_L}$	$F_{L,\min}$	$F_{L,\max}$	$\overline{M}$	$M_{\min}$	$M_{\max}$
		σ_{F_D}			σ_{F_L}			σ_M	
Units	$\times 10^7 N$						$\times 10^8 N \cdot m$		
CFD/CSD	7.4	6.65	8.75	0.02	-5	5.15	-0.2	-2.14	1.23
		0.5			1.7			0.7	
RWDI (1999)	6.8	3.5	10	-0.6	-8.6	7.4	0.1	-3.9	4.1
		0.88 *			2.28 *			1.14 *	

* estimated by: $(Maximum - Mean)/g$, where $g = 3.5$ is peak factor

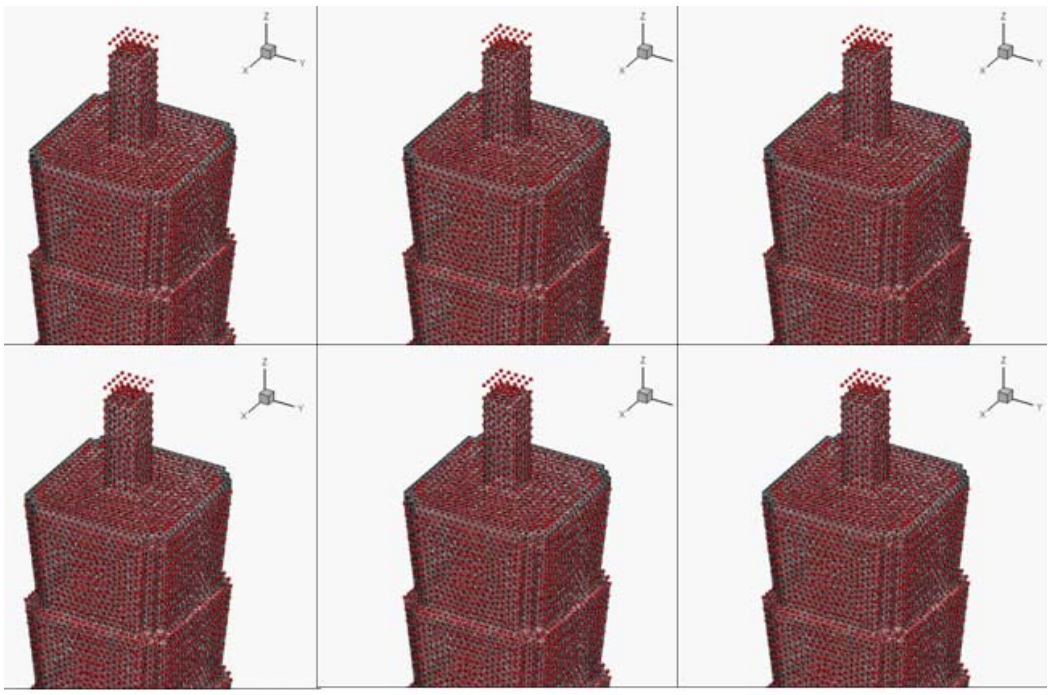

Fig.8 The matched mesh of CFD and CSD during the computations of FSI

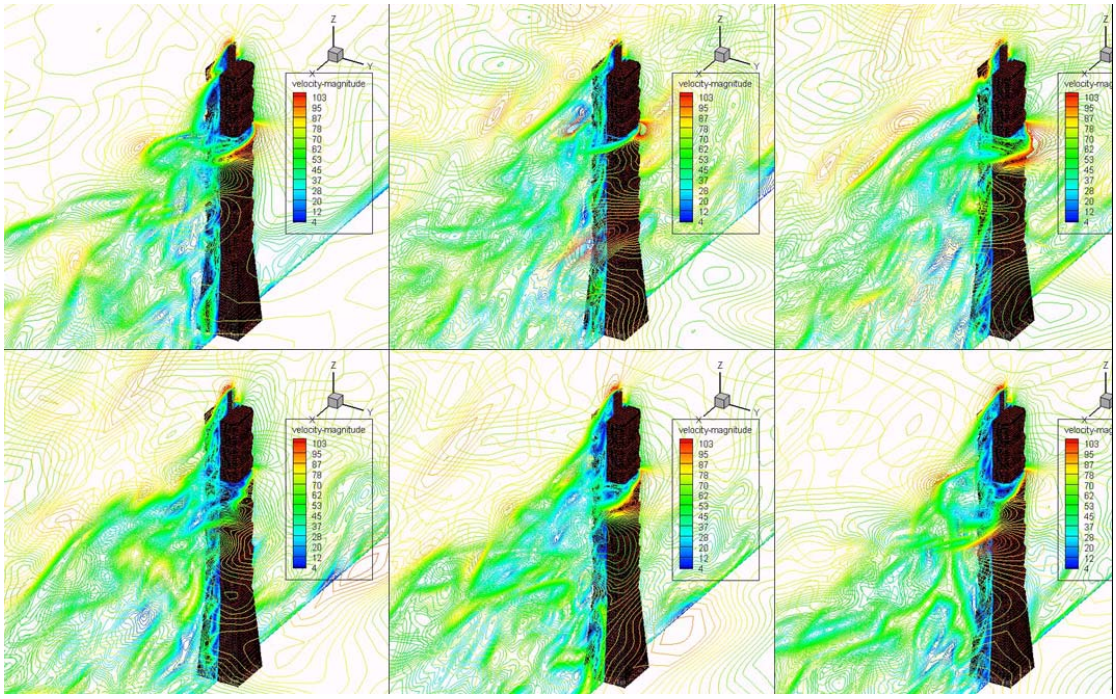

Fig.9 The coupled fluid and structure movement during the computations of FSI

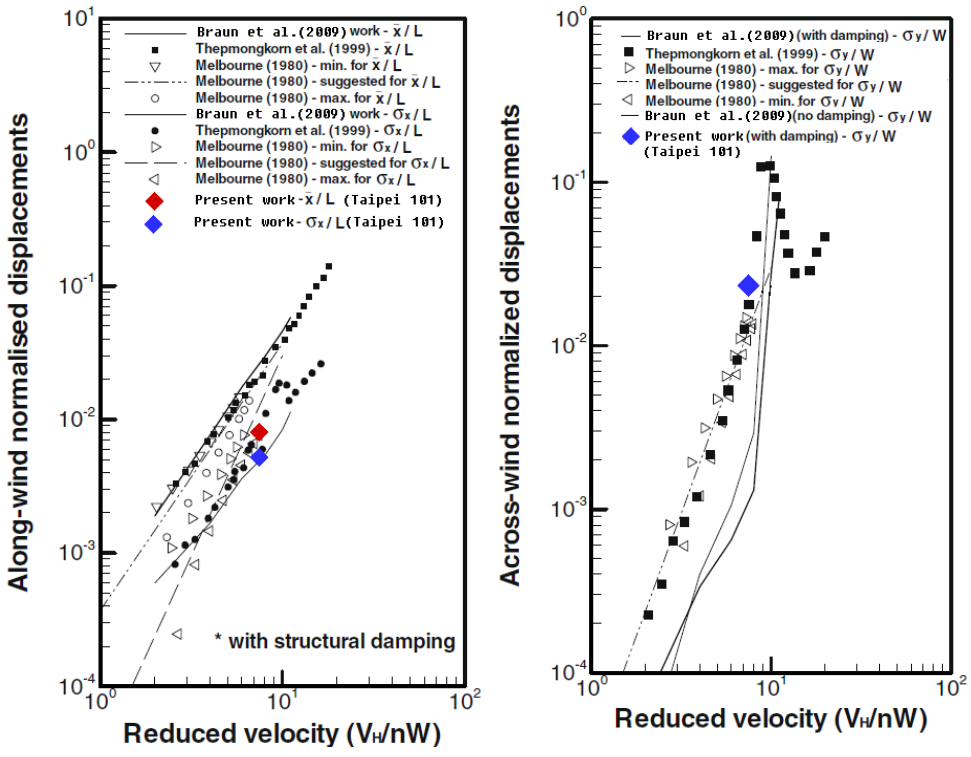

Fig.10 Comparison of along-wind and across-wind normalized displacements as functions of the reduced velocity with available data

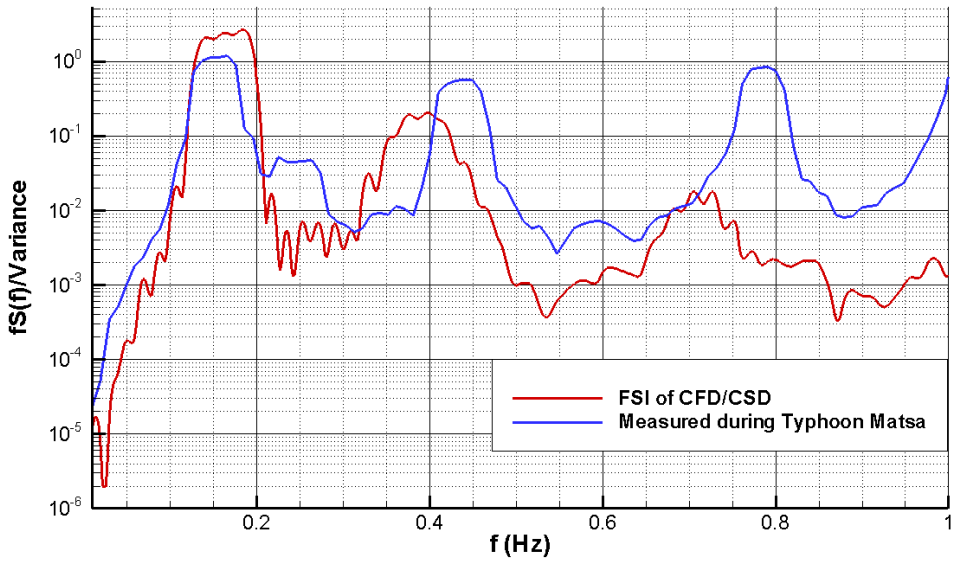

(a) along wind acceleration spectral

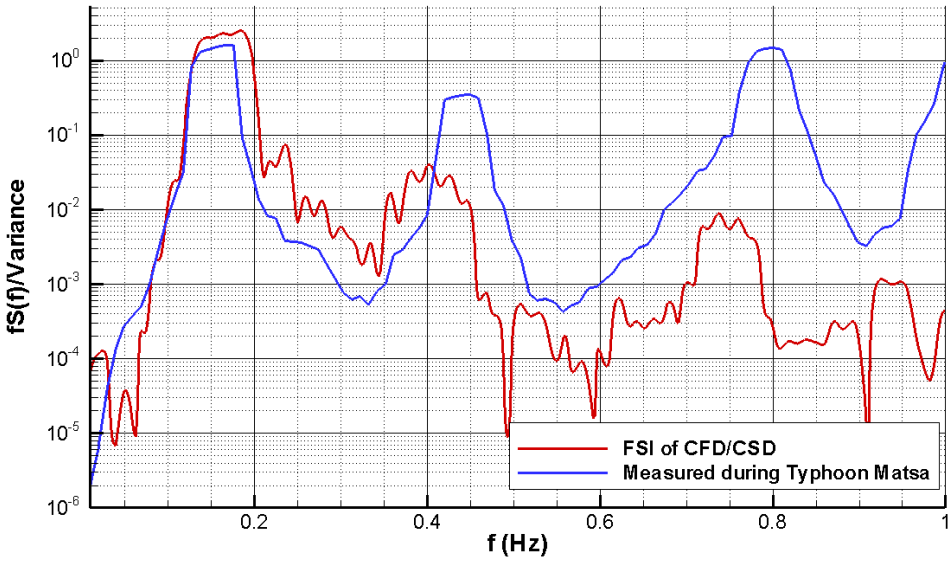

(a) across wind acceleration spectral

Fig.11 spectral comparison of acceleration with measured data of Li etal.(2011)

4. CONCLUSION

Combined with the methods and models suitable for relative coarse grid situations and simulation of high Reynolds number flows developed by authors recently, a parallel fluid-structure interaction method based on socket parallel architecture was established for large eddy simulation on wind flows around high-rise buildings. The aim of such developments is to obtain a combined method with capacity of high-efficiency two-way coupling between detailed fluid dynamics computing and solid structure dynamics computing so that the detailed wind induced responses for high-rise buildings can be resolved

practically. The 1:375 CAARC building model with Re=70000 and a full scale Taipei101 high-rise building with Re=1e8 are chosen as validation cases. The results obtained show that:

(1) The proposed FSI method can exchange a right loads and response information between CSD solver and CFD solver, so that the both nodes of CFD and CSD move and deform accordantly.
(2) Unlike ordinary two way coupling method, the proposed FSI method only exchange the integrated information of FSI interface, leading to greatly promotion of FSI efficiency; Besides, Different mesh styles and different operating platforms can be adopted by CFD solver and CSD solver respectively due to cross platform nature of socket communication.
(3) Both results of CAARC and Taipei101 building agree well with available experimental and numerical data, checking the accuracy and effectiveness of the proposed method and models.

Acknowledgements

The work described in this paper was fully supported by a key grant from National Natural Foundation of China (Project No. 90815030).

5. REFERENCES

[1] Fang Pingzhi, Gu Ming. (2008), "Numerical simulation of vortex-induced vibration for a square cylinder at high reynolds number," *Journal of Tongji University*, **36(2)**, 161-165(in Chinese).
[2] Huang, S.H., Li, Q.S. (2010b), "A new dynamic one-equation subgrid-scale model for large eddy simulations," *International Journal for Numerical Methods in Engineering,* **81**, 835–865.
[3] Huang, S.H., Li, Q.S., Wu, J.R., (2010a), "A general inflow turbulence generator for large eddy simulation," J. Wind Eng. Ind. Aerodyn., **98**, 600–617.
[4] Kajishima T, Nomachi T. (2006), "One-equation subgrid scale model using dynamic procedure for the energy production," J*ournal of Applied Mechanics*, Transactions ASME, 73, 368-373.
[5] Kataoka H. (2008), "Numerical simulations of a wind-induced vibrating square cylinder within turbulent boundary layer,"*Journal of Wind Engineering and Industrial Aerodynamics* , **96 (10-11)**, 1985 – 1997.
[6] Kim WW, Menon S. (1995), "A new dynamic one-equation subgrid-scale model for large eddy simulations," *AIAA-95-0356*.
[7] Melbourne WH. (1980), "Comparison of measurements on the CAARC standard tall building model in simulated model wind flows," J *Journal of Wind Engineering and Industrial Aerodynamics*,**6(1–2)**, 73–88.
[8] Nicoud F, Ducros F. (1999), "Subgrid-scale stress modeling based on the square of the velocity gradient tensor flow," *Turbulence and Combustion*, 62,183–200.

[9] Okamoto M, Shima N.(1999), “Investigation for the one-equation-type subgrid model with eddy-viscosity expression including the shear-dumping effect,” *JSME International Journal Series B*, 42,154–161.
[10] Q.S. Li, Y.Q Xiao, C.K Wong (2005), “Full-scale monitoring of typhoon effects on super tall buildings,” *Journal of Fluids and Structures*, **20**, 697–717.
[11] Q.S.Li,Lun-Hai Zhi,Alex Y Tuan, Chin-Sheng Kao,Sheng-Chung Su, and Chien-Fu Wu (2011), “Dynamic Behavior of Taipei 101 Tower: Field Measurement and Numerical Analysis,” *Journal of Structural Engineering*, 137(1)
[12] Revuz J, Hargreaves D M, Owen J S. (2009), “Numerical Simulation of the Dynamic Wind Loading on and Response of Tall Buildings,” EACWE 5 Florence, Italy.
[13] Shiau BS. (2000), “Velocity spectra and turbulence statistics at the northeastern coast of Taiwan under high-wind conditions,” *Journal of Wind Engineering and Industrial Aerodynamics*,**88**,139-151.
[14] Smirnov, R., Shi, S., and Celik, I. (2001), “Random flow generation technique for large eddy simulations and particle-dynamics modeling,” *Journal of Fluids Engineering*. **123**, 359-371
[15] Su Guo, Chen Shuifu, Tang Jinchun (2008), “Numerical analysis on physical mechanism of flexible high-rise's unstable aeroelastic phenomena in cross-wind,” *Journal of Jiangnan University*, **7(2)**, 227-233 (in Chinese).
[16] Swaddiwudhipong S, KHAN M S. (2002), “Dynamic response of wind-excited building using CFD,” *Journal of Sound and Vibration*, **253(4)**, 735- 754
[17] Tamura T , Itoh Y. (1999b), “Unstable aerodynamic phenomena of a rectangular cylinder with critical section,” *Journal of Wind Engineering and Industrial Aerodynamics*, **83 (1-3)**, 121-133
[18] Tamura T, Itoh Y. (1997), “Three-dimensional vortical flows around a bluff cylinder in unstable oscillations,” *Journal of Wind Engineering and Industrial Aerodynamics*, **67-68**,141-154.
[19] Tamura T, Ono Y.(2003), “LES analysis on aeroelastic instability of prisms in turbulent flow,” *Journal of Wind Engineering and Industrial Aerodynamics*, **91(12)**, 1827–1846.
[20] Tamura T. (1999a), “Reliability on CFD estimation for wind-structure interaction problems,” *Journal of Wind Engineering and Industrial Aerodynamics*, **81(1-3)**,117-143.
[21] Tamura T., (2008), “Towards practical use of LES in wind engineering,” *Journal of Wind Engineering and Industrial Aerodynamics*, **96**,1451–1471.
[22] Thepmongkorn S, Kwok KCS, Lakshmanan N. (1999), “A two-degree-of-freedom base hinged aeroelastic (BHA) model for response predictions,” *Journal of Wind Engineering and Industrial Aerodynamics*, **83**,171–81.
[23] Wind-induced structural responses cladding wind load study, Roman Williams Davies & Irwin Inc (RWDI), 1999.